A model for the alternating phase lags associated with QPOs in X-ray binaries

M. Böttcher[1][2], E. P. Liang[2]

ABSTRACT

We present a theoretical model for the alternating phase lags associated with QPO fundamental and harmonic frequencies observed in some Galactic black-hole candidates. We assume that the accretion flow exhibits a transition from an outer cool, optically thick accretion disk to a hot, inner advection-dominated accretion flow (ADAF), and that the QPOs are related to small-scale oscillations of the accretion rate and the transition radius. We present an analytical estimate of the expected phase lags at the fundamental and first harmonic frequencies of the QPOs and perform detailed time-dependent Monte-Carlo simualtions of the radiation transport in the oscillating ADAF / cool disk system. We find that this model is well suited to reproduce alternating phase lags between the fundamental and the first harmonic. It also naturally explains the trend observed in GRS 1915+105 that, as the soft X-ray luminosity increases, the QPO frequency increases and the phase lag associated with the QPO fundamental frequency changes sign from positive to negative. The relation between the disk temperature and the QPO frequency observed in GRS 1915+105 is consistent with a secular instability modulating the disk evaporation at the transition radius.

Subject headings: X-rays: stars — accretion, accretion disks — black hole physics — radiative transfer — radiation mechanisms: thermal

1. Introduction

The steadily increasing amount of high-quality, high time-resolution X-ray data from Galactic X-ray binaries, has stimulated vital interest in the characteristics of the rapid variability of these objects. The X-ray emission from both Galactic black-hole candidates (GBHCs) and accreting neutron stars is known to vary on a wide range of time scales, sometimes showing quasi-periodic oscillations (QPOs) (for reviews see, e.g., van der Klis 1995, Cui 1999a). In GBHCs, such QPOs have been detected at frequencies ranging from several mHz to $\lesssim 100$ Hz. These QPOs are most

---

[1]Chandra Fellow

[2]Rice University, Space Physics and Astronomy Department, MS 108
6100 S. Main Street, Houston, TX 77005 – 1892, USA

notable when the sources are in the low-hard or in the rare very high state. Recently, correlations between the amplitudes and centroid frequencies of several types of QPOs with the spectral characteristics of the source have been found in some objects (Rutledge et al. 1999, Markwardt, Swank, & Taam 1999, Sobczak et al. 1999, Muno, Morgan & Remillard 1999). A general pattern emerging from these analyses is that the frequency of those types of QPOs which do show a correlation with spectral properties, seems to increase with both the power-law and the disk black-body flux from the source.

A surprising property of some types of QPOs has recently been found in the 67 mHz QPO of GRS 1915+105 (Cui 1999b), the 0.5 – 10 Hz QPO of the same source (Reig et al. 2000, Lin et al. 2000), and in the 0.3 – 3 Hz QPO in XTE J1550-564 (Cui, Zhang, & Chen 2000): While the phase lag at the QPO fundamental frequency is negative, the phase lag associated with the first harmonic was positive. In the case of the low-frequency QPO of GRS 1915+105, even three harmonics were detected, and the phase lags were found to alternate between subsequent harmonics (Cui 1999b). The phase lag associated with the 0.5 – 10 Hz QPO of GRS 1915+105 was found to change sign from positive to negative as the QPO frequency increases above ~ 2.5 Hz (Reig et al. 2000, Lin et al. 2000).

These peculiar patterns are apparently completely counter-intuitive in the light of currently discussed models for the hard phase lags in X-ray binaries. Models proposed to explain the hard phase lags are either based to the energy-dependent photon escape time in Compton upscattering scenarios for the production of hard X-rays (Kazanas, Hua & Titarchuk 1997, Böttcher & Liang 1998), or due to intrinsic spectral hardening during X-ray flares, e.g. due to decreasing Compton cooling in active regions pushed away from an underlying accretion disk in a patchy-corona model (Poutanen & Fabian 1999) or due to density perturbations drifting inward through an ADAF toward the event horizon (Böttcher & Liang 1999). These models dealt only with the continuum variability and did not consider the effects of QPOs.

In this paper we will explore the response of a two-phase accretion flow, consisting of an outer, cool, optically thick accretion disk and an inner, hot ADAF (Narayan & Yi 1994, Abramowicz et al. 1995, Chen et al. 1995), to a periodically varying soft photon input from the cool disk (Liang & Böttcher 2000). A two-phase accretion flow with an inner ADAF has been found to produce good fits to the photon spectra of, e.g., several Galactic X-ray binaries (e.g., Narayan, McClintock & Yi 1996, Hameury et al. 1997, Esin et al. 1998), low-luminosity AGN (Quataert et al. 1999) and giant elliptical galaxies (Fabian & Rees 1995, di Matteo & Fabian 1997, di Matteo et al. 2000). In §2, we describe the basic model setup according to this two-phase accretion flow, and derive an analytical estimate for the expected phase lags associated with the QPO and the first harmonic applicable in some simplified cases. A short description of the Monte-Carlo simulations used to solve the time-dependent radiation transport problem follows in §3. In §4 we describe a series of simulations designed specifically to explain the peculiar phase lag behavior associated with the 0.5 – 10 Hz QPO in GRS 1915+105. We summarize in §5.

2. Model setup and analytical estimates

The basic model setup, as motivated in the introduction, assumes that the inner portion of the accretion flow is described by an ADAF, where the density profile is approximately given by a free-fall profile, $n_e(r) \propto r^{-3/2}$, and the electron temperature is close to the virial temperature and thus scales as $T_e(r) \propto r^{-1}$. We emphasize, however, that other hot two-temperature inner disk models would give similar results. The ADAF exists out to a transition radius R_{tr}, beyond which the flow is organized in a standard optically thick, geometrically thin Shakura-Sunyaev disk (Shakura & Sunyaev 1973). The transition radius is typically expected to be several $100 \, R_s \lesssim R_{\mathrm{tr}} \lesssim 10^4 \, R_s$ (Honma 1996, Manmoto et al. 2000, Meyer et al. 2000), where R_s is the Schwarzschild radius. Outside this transition radius, the disk temperature scales as $T_D(r) \propto r^{-3/4}$. With the free-fall density profile given above, the radial Thomson depth of the corona may be written as $\tau_T^{\mathrm{ADAF}} = 0.71 \, \dot{M}_{17}/(m \, r_i^{1/2})$, where $\dot{M}_{17}$ is the accretion rate through the ADAF in units of 10^{17} g s^{-1}, m is the mass of the central compact object in units of solar masses, and r_i is the inner edge of the ADAF in units of Schwarzschild radii.

The basic assumption of our baseline model is that the observed QPOs in the X-ray variability of Galactic black-hole candidates are related to small-scale oscillations of the transition radius. Such oscillations in r_{tr} may be caused by variations of the accretion rate, but we defer a detailed study of possible mechanisms driving the oscillations to a later paper. We thus assume that, as a function of time t, the transition radius oscillates as $R_{\mathrm{tr}}(t) = r_{\mathrm{tr}} \, (1 + a_r \, \sin[\omega t])$, where $a_r \ll 1$ is the amplitude of the oscillation and $\omega = 2\pi f_{\mathrm{QPO}}$ the QPO frequency. Denoting $\xi \equiv 1 + a_r \, \sin(\omega t)$, the time-dependent disk flux may then be estimated as $F_D(t) \propto [R_{\mathrm{tr}}(t)]^2 \, [T_d(t)]^4 \propto (r_{\mathrm{tr}} \, \xi)^{-1}$. In the following, we are focusing on an analytical description of the X-ray signals at the QPO fundamental and first harmonic frequencies. Thus, we will expand all expressions up to the 2nd order in $a_r \sin(\omega t)$. For the disk flux, this yields

$$F_D(t) \approx F_{D,0} \left[1 + \frac{a_r^2}{2} - a_r \, \sin(\omega \, t) - \frac{a_r^2}{2} \, \cos(2\omega \, t) \right]. \tag{1}$$

The disk spectrum is approximately a blackbody spectrum at the temperature of the disk at the transition radius, and for the purpose of a simple analytical estimate, we assume that it is monochromatic at a disk photon energy $E_D(t) \propto T_D(r_{\mathrm{tr}}) \propto (r_{\mathrm{tr}} \, \xi)^{-3/4}$. For any observed photon energy E, we define the ratio

$$\epsilon(t) \equiv E/E_D(t) \equiv \epsilon_0 \, \xi^{3/4}. \tag{2}$$

Now, at any given time, a fraction $f_c \approx \frac{1}{2} \left(1 - \frac{\pi}{4} \right)$ of the disk radiation will intercept the quasi-spherical inner ADAF-like corona and serve as soft seed photons for Compton upscattering, producing the time-variable hard X-ray emission. Note that additional hard X-ray emission will be produced by Comptonization of synchrotron and bremsstrahlung photons produced in

the inner portions of the ADAF. However, since we do not assume significant changes of the structure of the inner ADAF in the course of the small-scale oscillations of the transition radius, this internal synchrotron and bremsstrahlung emission will constitute a quasi-DC flux component which does not contribute significantly to the variability properties of the source. Being mainly interested in the quasi-periodic variability, we do not consider this emission component here. The time-dependent Comptonization response function to the oscillating disk flux in this geometry can be parametrized as

$$h(t, \tau, \epsilon_0) = \Theta(u) \left\{ A\, u^{\alpha-1}\, e^{-u/\beta} + B\, u^{\kappa-1}\, \Theta\left(\frac{2\, R_{\mathrm{tr}}(\tau)}{c} - u\right)\right\} \tag{3}$$

(Böttcher & Liang 1998), where now t is the observing time, τ is the time of soft photon emission at the transition radius, $u \equiv t - \tau$, Θ is the Heaviside function, A and B are normalization factors which are generally energy and time dependent. In the general case, the indices α and κ, and the time "constant" β also depend on photon energy and time (β depends on time through the time-dependence of the extent of the corona and the disk photon energy).

The observable energy flux at time t at photon energy E is then given by

$$F(E, t) = f_d\, F_{\mathrm{D}}(E, t) + f_c \int\limits_{-\infty}^{t} d\tau \int\limits_{0}^{\infty} dE_{\mathrm{D}}\, F_{\mathrm{D}}(E_{\mathrm{D}}, \tau)\, h(t, \tau, \epsilon_0), \tag{4}$$

where $f_d \equiv 1 - f_c$. For the purpose of the analytical estimate, we now focus on two regimes for the observed photon energies. At low energies, close to the peak energy of the disk emission, the observed light curve will be dominated by the direct disk emission (the first term on the r.h.s. of Eq. 4) and the contribution from reflection in the outer regions of the ADAF, proportional to $B \approx c/(2R_{\mathrm{tr}}[\tau])$. For an ADAF-like density and temperature profile, we may set $\kappa = 1$, i. e. the reflection light curve is flat over the light crossing time through the corona. The multiple-scattering term, proportional to A in Eq. 3, may be neglected at low photon energies.

The observed signal at high photon energies, $E \gg E_{\mathrm{D}}$ will be dominated by the multiple-scattering term, i. e. we may set $B = 0$ for high-energy photons. Since multiple Compton scattering results in a power-law spectrum, we parametrize the energy dependence of the normalization of this term as $A = A_0\, \epsilon_0^{-\gamma}\, x^{-3\gamma/4}$, where γ is the photon spectral index of the Comptonized spectrum, and $x = 1 + \sin(\omega\tau)$. The parameter α is generally energy dependent. However, we find that a constant value of $\alpha = 10$ yields a reasonably good description of the multiple-scattering light curve for an ADAF-like temperature and density profile. To the same degree of approximation, we consider β as constant for a given energy channel, and note its scaling as $\beta \propto r_{\mathrm{tr}}$. Furthermore, β increases with photon energy. Now, using the δ function assumption for the disk spectrum in the integral in Eq. 4, the observed light curve reduces to

$$F(E,t) \approx f_d\, F_{\rm D}(E,t) + f_c\, F_{D,0} \int\limits_0^\infty du\, \left\{ A_0\, \epsilon_0^{-\gamma}\, x^{-\delta} u^{\alpha-1} e^{-u/\beta}\ +\ x^{-2} B_0(\epsilon_0)\, \Theta\left(\frac{2\,r_{\rm tr}}{c} - u\right) \right\}, \quad (5)$$

where $\delta \equiv (3\gamma/4) + 1$.

Expanding all terms up to the first harmonic and writing

$$\frac{F(E,t)}{F_{D,0}} = \eta_0 + \eta_1 \sin(\omega t) + \eta_2 \cos(\omega t) + \eta_3 \sin(2\omega\, t) + \eta_4 \cos(2\omega\, t) \qquad (6)$$

we find

$$\eta_0 = f_d\left(1 + \frac{a_r^2}{2}\right) + f_c\frac{B}{\omega}\,\phi_r\left(1 + \frac{3}{2}a_r^2\right) + f_c A_0 \epsilon_0^{-\gamma}\left(\beta^\alpha \Gamma[\alpha] + \frac{\delta[\delta+1]}{4}a_r^2\,[C_2(\alpha) + S_2(\alpha)]\right), \quad (7)$$

$$\eta_1 = -f_d\, a_r - 2\, f_c\frac{B}{\omega}a_r \sin\phi_r - f_c A_0\epsilon_0^{-\gamma}\delta a_r\, C_1(\alpha), \qquad (8)$$

$$\eta_2 = 2\, f_c\frac{B}{\omega}a_r\,(1 - \cos\phi_r) + f_c A_0\epsilon_0^{-\gamma}\delta a_r S_1(\alpha), \qquad (9)$$

$$\eta_3 = -\frac{3}{2}f_c\frac{B}{\omega}a_r^2 \sin^2\phi_r - \frac{1}{2}f_c A_0\epsilon_0^{-\gamma}\delta(\delta+1)\, a_r^2 SC(\alpha), \qquad (10)$$

$$\eta_4 = -\frac{1}{2}f_d\, a_r^2 - \frac{3}{2}f_c\frac{B}{\omega}a_r^2\,\sin\phi_r\,\cos\phi_r + \frac{1}{4}f_c A_0\epsilon_0^{-\gamma}\delta(\delta+1)\, a_r^2(S_2[\alpha] - C_2[\alpha]), \qquad (11)$$

where $\phi_r \equiv \frac{2\omega}{c}\, r_{\rm tr}$, and we have defined the integrals

$$S_1(\alpha) \equiv \int\limits_0^\infty du\, u^{\alpha-1}e^{-u/\beta}\sin(\omega u) = \beta^\alpha \Gamma(\alpha)\frac{\sin(\alpha \arctan[\beta\omega])}{(1 + [\beta\omega]^2)^{\alpha/2}}, \qquad (12)$$

$$C_1(\alpha) \equiv \int\limits_0^\infty du\, u^{\alpha-1}e^{-u/\beta}\cos(\omega u) = \beta^\alpha \Gamma(\alpha)\frac{\cos(\alpha \arctan[\beta\omega])}{(1 + [\beta\omega]^2)^{\alpha/2}}, \qquad (13)$$

$$S_2(\alpha) \equiv \int\limits_0^\infty du\, u^{\alpha-1}e^{-u/\beta}\sin^2(\omega u) = \frac{\beta^\alpha \Gamma(\alpha)}{2}\left\{1 - \frac{\cos(\alpha \arctan[2\,\beta\omega])}{(1 + [2\,\beta\omega]^2)^{\alpha/2}}\right\}, \qquad (14)$$

$$C_2(\alpha) \equiv \int\limits_0^\infty du\, u^{\alpha-1}e^{-u/\beta}\cos^2(\omega u) = \frac{\beta^\alpha \Gamma(\alpha)}{2}\left\{1 + \frac{\cos(\alpha \arctan[2\,\beta\omega])}{(1 + [2\,\beta\omega]^2)^{\alpha/2}}\right\}, \qquad (15)$$

$$SC(\alpha) \equiv \int\limits_0^\infty du\, u^{\alpha-1}e^{-u/\beta}\sin(\omega u)\cos(\omega u) = \frac{\beta^\alpha \Gamma(\alpha)}{2}\frac{\sin(\alpha \arctan[2\,\beta\omega])}{(1 + [2\,\beta\omega]^2)^{\alpha/2}}. \qquad (16)$$

Defining the phases, relative to the R_{tr} oscillation, of the signal in a given energy band at the QPO frequency and the first harmonic, respectively, by

$$F(t) = \eta_0 + \xi_1 \sin(\omega t + \Delta_Q) + \xi_2 \sin(2\omega\, t + \Delta_H) \tag{17}$$

with $\tan \Delta_Q = \eta_2/\eta_1$ and $\tan \Delta_H = \eta_4/\eta_3$, we find for a low-energy channel (with mean energy close to the peak energy of the disk emission spectrum):

$$\tan \Delta_Q(\mathrm{LE}) \approx -\frac{2\, f_c \frac{B}{\omega}\, (1 - \cos \phi_r)}{2\, f_c \frac{B}{\omega}\, \sin \phi_r + f_d}, \tag{18}$$

$$\tan \Delta_H(\mathrm{LE}) \approx \frac{f_d + \frac{3}{2}\, f_c \frac{B}{\omega}\, \sin(2\phi_r)}{\frac{3}{2}\, f_c \frac{B}{\omega}\, (1 - \cos[2\phi_r])}. \tag{19}$$

Assuming that the direct disk emission ($\propto f_d$) is strongly dominating at this energy, and that both η_3 and η_4 are negative in this case, we have $\Delta_Q(\mathrm{LE}) \approx 0$, and $\Delta_H(\mathrm{LE}) \approx -\pi/2$.

For high photon energies, dominated by multiple Compton scattering, we find

$$\Delta_Q(\mathrm{HE}) = -\alpha \arctan(\beta\omega) + k_0 \pi, \tag{20}$$

$$\Delta_H(\mathrm{HE}) = \alpha \arctan(2\,\beta\omega) + k_1 \pi, \tag{21}$$

where $k_i \in (0, -1, 1)$ are determined by the signs of $\eta_1, \ldots, \eta_4$. With the definition of the phases Δ in Eq. 17, the phase lags are given by $\Delta\phi = \Delta(\mathrm{LE}) - \Delta(\mathrm{HE})$. Throughout this paper we adopt the convention that positive phase and time lags correspond to hard photons lagging the soft ones.

Intuitively, phase and time lags between the disk-radiation dominated low-energy photons and the Compton-upscattering dominated high-energy photons are determined by the ratio between the QPO period T_{QPO} and the time required for soft photons to reach the inner ADAF region and be Compton upscattered to hard X-ray energies. If this light-travel and diffusion time is *longer than half a QPO period, but less than the QPO period itself*, the phase lag at the QPO fundamental frequency — which physically is still a hard lag — appears as a *soft lag* due to the periodicity of the light curves. The same argument holds for the nth harmonic of the QPO, where the period now corresponds to $1/(n+1)$ of the QPO fundamental period.

For a very large transition radius, the direct disk emission may not contribute significantly to the X-ray flux. In that case, the phase lag between two energy channels will be dominated by the difference in diffusion time scales β, and we expect

$$\Delta\phi_{\mathrm{QPO}} \approx \alpha(\arctan[\beta_j\omega] - \arctan[\beta_i\omega]), \tag{22}$$

$$\Delta\phi_{1.\ \mathrm{harm.}} \approx \alpha(\arctan[2\beta_i\omega] - \arctan[2\beta_j\omega]). \tag{23}$$

for two energy channels $E_i < E_j$.

3. Monte Carlo simulations

The estimates derived in the previous section were based on several major simplifications in order to keep the problem analytically trackable. In order to test the validity of our approximations and to provide results under more realistic assumptions, we have simulated the radiation transfer in our oscillating ADAF/disk model system, using our time-dependent Monte-Carlo Comptonization code. For a detailed description of the code and its capabilities, see Böttcher & Liang (1998, 1999).

In our simulations, we approximate the accretion disk emission by a blackbody spectrum with the temperature of the disk inner edge at any given time, and its time-dependent luminosity determined as described in the previous section. A fraction f_c of the time dependent disk emission enters the spherical Comptonizing region at its outer boundary and serves as seed photon field for Comptonization. The ADAF is characterized by an $r^{-3/2}$ density and r^{-1} temperature structure, and the electron temperature is normalized to $kT_e(R_s) = 500$ keV, i. e. the electrons become relativistic at the event horizon. The event horizon is treated as an absorbing inner boundary. The corona has the specified radial Thomson depth of $\tau_{\mathrm{T}}^{\mathrm{ADAF}}$ when the ADAF/disk transition is located at r_{tr}. As r_{tr} oscillates, we leave the density and temperature structure of the ADAF inside $R_{\mathrm{tr}}(t)$ unchanged and set the coronal electron density equal to zero outside $R_{\mathrm{tr}}(t)$.

The resulting light curves, generally consisting of the sum of direct disk emission and the Comptonized emission from the corona, are sampled in 5 photon energy bins and over 512 time steps of $\Delta t \lesssim 0.05\,T_{\mathrm{QPO}}$. For several test cases, we have run identical problem simulations with different time steps, in order to verify that our results are independent of the time step chosen. The energy-dependent light curve are then Fourier transformed, using an FFT algorithm (Press et al. 1992), and the power density spectra and phase lags are calculated.

In order to test our Monte Carlo code against the analytical estimates derived in the previous section, we did a series of simulations in which the accretion disk temperature at the equilibrium transition radius and the QPO frequency were artificially chosen artificially constant among different simulations, and at a value such that the emission in the $2 - 5$ keV reference channel was always dominated by direct disk emission, while the highest two energy channels ($15 - 40$ keV and $40 - 100$ keV, respectively) were dominated by Compton-upscattered radiation from the corona. In that case, Eqs. (18) – (21) with constant values of α and β/r_{tr} may be used in order to approximate the expected phase lags. In Fig. 1, the phase lags at the QPO fundamental and first harmonic frequencies as measured in our simulations are compared to these analytic estimates. The figure demonstrates that the two approaches are in excellent agreement, indicating that our numerical procedure reliably reproduces the time-dependent radiation transport properties of the model system.

4.   The $0.5 - 10$ Hz QPOs in GRS 1915+105

As briefly mentioned in the introduction, the variable-frequency QPO at $0.5 - 10$ Hz observed in the low-hard state of GRS 1915+105 exhibits a very peculiar phase lag behavior (Reig et al. 2000, Lin et al. 2000): If the source has a rather hard (photon index $\gamma \lesssim 2.7$) photon spectrum and low X-ray flux, the QPO frequency is low $f_{\rm QPO} \lesssim 2$ Hz, and the phase lags associated with both the QPO fundamental and the first harmonic frequencies are positive. As the X-ray flux increases and the photon spectrum becomes softer, the QPO centroid frequency increases, and the phase lag at the QPO fundamental frequency decreases and changes sign at $f_{\rm QPO} \sim 2.5$ Hz. At the same time, the phase lag associated with the first harmonic frequency increases. As the source becomes more X-ray luminous and the spectrum becomes softer, the QPO frequency increases up to ~ 10 Hz, and the phase lag associated with the QPO fundamental continues to decrease, while the phase lag at the first harmonic frequency remains positive and does not show any obvious correlation with spectral parameters or the QPO frequency. Spectral fits to GRS 1915+105 with a disk blackbody + power-law model to different spectra states along this sequence revealed that the inner disk temperature increases from ~ 0.7 keV to ~ 1.5 keV as the QPO frequency increases from 0.5 to 10 Hz (Muno et al. 1999).

In order to model this behavior, we parametrize the disk temperature at the transition radius, $T_{\rm D}(r_{\rm tr})$, and the QPO frequency as power-laws in $r_{\rm tr}$. Assuming $T_{\rm D}(r_{\rm tr}) \propto r_{\rm tr}^{-3/4}$, a simple power-law relation spanning the observed ranges of $0.7\,{\rm keV} \leq kT_{\rm D} \leq 1.5\,{\rm keV}$ and $0.5\,{\rm Hz} \leq f_{\rm QPO} \leq 10\,{\rm Hz}$ (Muno et al. 1999) yields a scaling $f_{\rm QPO} \propto T_{\rm D}^4 \propto r_{\rm tr}^{-3}$. This scaling may indicate that the transition radius oscillations are related to a modulation of the disk evaporation process, responsible for the transition to the inner ADAF, by a secular instability. The frequency of such modulations might be proportional to the inverse of the evaporation time scale, $\tau_{\rm evap}^{-1}$, which is expected to be proportional to the disk surface flux, $dL/dA \propto T_{\rm D}^4 \propto r_{\rm tr}^{-3}$. Thus, the assumed scaling laws of the disk temperature and QPO frequency with the transition radius are physically plausible.

For the high-QPO-frequency end of the sequence mentioned above, we choose a transition radius of $r_{\rm tr} = 6 \cdot 10^8$ cm, corresponding to $\sim 700\,R_s$ for a $3\,M_\odot$ black hole or the theoretical limit of $340\,R_s$ found by Meyer et al. (2000) for a $\sim 6\,M_\odot$ black hole (unfortunately, the mass of the central object in GRS 1915+105 is not known due to the lack of an optical counterpart). The QPO frequency (i.e. the transition-radius oscillation frequency) is 10 Hz, and the disk temperature at the transition radius is 1.5 keV. Assuming $M = 6\,M_\odot$ and $r_{tr} = 340\,R_s$, this is in agreement with the cool, gas-pressure dominated disk model for $\alpha^{-1/5}\,(L/0.057 L_{\rm Edd})^{3/10} \sim 1$, where α is the viscosity parameter.

Using the Monte-Carlo simulations described in the previous section, we calculate the photon-energy dependent light curves, Fourier transform them, and calculate the Fourier-frequency dependent phase lags from the cross-correlation functions. For comparison with the results of Lin et al. (2000) we sample the light curves in the energy channels $0.1 - 3.3$ keV [1], $3.3 - 5.8$ keV

[2], 5.8 – 13 keV [3], 13 – 41 keV [4], and 41 – 100 keV [5], and focus on the phase lags between channels [4] and [2]. We perform a series of 6 simulations, each with different values of $r_{\rm tr}$, implying different QPO frequencies and disk temperatures according to the scaling laws quoted above.

Two representative examples of the resulting power and phase lag spectra are shown in Figs. 2 and 3 for a high-frequency (6.7 Hz) case with alternating phase lags and a low-frequency (1.1 Hz) case with positive phase lags at both fundamental and first harmonic frequencies, respectively.

The results of the complete series of simulations are listed in Table 1 and illustrated in Fig. 4. From Fig. 4 we see that this model reproduces the key features of the peculiar QPO phase lag behavior observed in GRS 1915+105, in particular the change of sign of the phase lag associated with the QPO as the QPO centroid frequency increases, and the alternating phase lags between QPO fundamental and first harmonic at high QPO frequencies. We point out that the measured values of the hard lags at the first harmonic frequency for $f_{\rm QPO} \gtrsim 2$ Hz are significantly smaller than predicted by our model. However, this is expected because, for realistic signal-to-noise ratios, the (random-phase) Poisson noise contaminating the actual data always suppresses high phase lag values, but leaves small values of $|\Delta\phi|$ almost unaffected (Zhang 2000, private communication).

Table 1 and Fig. 4 also show the predicted phase lags at the second harmonic of the QPO, which has not been observed yet. We expect that, if a second harmonic is found in any future or archived observation of GRS 1915+105, it should be associated with a negative phase lag, at least for $f_{\rm QPO} \gtrsim 2$ Hz.

We need to point out that the more complicated case discussed in this section is not directly comparable to the test cases illustrated in Fig. 1 since we are now varying the accretion disk temperature and the QPO frequency when varying the transition radius. This also changes the parameters α and β entering the analytical estimates as a function of $r_{\rm tr}$ in a non-trivial way.

5.   Summary and conclusions

We have investigated the time-dependent X-ray emission from an oscillating two-phase accretion flow, consisting of an outer, cool, optically thin accretion disk, and an inner ADAF. Based on this model, we are proposing an explanation for the peculiar phase lag behavior associated with the variable-frequency 0.5 – 10 Hz QPOs observed in GRS 1915+105. In particular, the changing sign of the phase lag at the QPO fundamental frequency as the QPO frequency increases, and the alternating phase lags between QPO fundamental and first harmonic frequencies in the case of a high QPO frequency are well reproduced by this model. The relation between QPO frequency, transition radius and inner disk radius can be interpreted physically, if the QPO is triggered by a modulation of the transition radius by a secular instability affecting the disk evaporation responsible for the disk/ADAF transition. Based on our results for GRS 1915+105, we predict that, if a second harmonic to the variable-frequency QPO at $f_{\rm QPO} \gtrsim 2$ Hz is detected, it should be associated with a negative phase lag.

We found that oscillations at the transition radius can naturally lead to apparent soft lags associated with the QPO frequency, if the photon diffusion time related to the production of hard X-rays is longer than half a QPO period. We point out that it is very unlikely that the same mechanism is responsible for the alternating phase lags observed in the 67 mHz QPOs and its harmonics since this would require a transition radius at $r_{tr} \gtrsim 10^5 R_s$. This large size of the ADAF is implausible for a non-quiescent state. The 67 mHz QPO alternating phase lag pattern has been observed in a high-flux state of GRS 1915+105, in which we would generally expect the disk to extend down to rather small radii.

One caveat of the model we have proposed here is that it requires a rather large accretion rate in order to produce the observed disk luminosity from GRS 1915+105. This, in turn, requires either that a large fraction of the accreted mass is lost to the collimated outflow of the radio jets, or that the ADAF has a very low radiative efficiency in order not to overproduce the hard power-law emission from the hot ADAF. However, since GRS 1915+105 is known to have very powerful, superluminal radio jets (Mirabel & Rodríguez 1994), it is plausible to assume that, indeed, a significant fraction of the mass accreted through the outer disk is not advected through the ADAF, but is powering the radio jets.

REFERENCES

Abramowicz, M. A., Chen, X., Kato, S., Lasota, J.-P., & Regev, O., 1995, ApJ, 438, L37

Böttcher, M., & Liang, E. P., 1998, ApJ, 506, 281

Böttcher, M., & Liang, E. P., 1999, ApJ, 511, L37

Chen, X., Abramowicz, M. A., Lasota, J.-P., et al. 1995, ApJ 443, L61

Cui, W., 1999a, in ASP Conf. Ser., 161, High Energy Processes in Accreting Black Holes, eds. J. Poutanen & R. Svensson (San Francisco: ASP), 97

Cui, W., 1999b, ApJ, 524, L59

Cui, W., Zhang, S. N., & Chen, W., 2000, ApJ, 531, L45

di Matteo, T., & Fabian, A. C., 1997, MNRAS, 286, L50

di Matteo, T., Quataert, E., Allen, S. W., Narayan, R., & Fabian, A. C., 2000, MNRAS, 311, 507

Esin, A. A., Narayan, R., Cui, W., Grove, J. E., & Zyang, S. N., 1998, ApJ, 505, 854

Fabian, A. C., & Rees, M. J., 1995, MNRAS, 277, L55

Hameury, J.-M., Lasota, J.-P., McClintock, J. E., & Narayan, R., 1997, ApJ, 489, 234

Honma, F., 1996, PASJ, 48, 77

Kazanas, D., Hua, X.-M., & Titarchuk, L. 1997, ApJ 480, 735

Liang, E. P., & Böttcher, M., 2000, in preparation

Lin, D., Smith, I. A., Liang, E. P., & Böttcher, M., 2000, ApJ, submitted

Manmoto, T. Kato, S., Nakamura, K. E., & Narayan, R., 2000, ApJ, 529, 127

Meyer, F., Liu, B. F., & Meyer-Hofmeister, E., 2000, A&A, 354, L67

Mirabel, I. F., & Rodríguez, L. F., 1994, Nature, 371, 46

Muno, M. P., Morgan, E. H., & Remillard, R. A., 1999, ApJ, 527, 321

Narayan, R., & Yi, I. 1994, ApJ 428, L13

Narayan, R., McClintock, J. E., & Yi, I., 1996, ApJ, 457, 821

Poutanen, J., & Fabian, A. C., 1999, MNRAS, 306, L31

Press, W. H., Teutolski, S. A., Vetterling, W. T., & Flannery, B. P., 1992, "Numerical Recipes in C", Cambridge University Press

Quataert, E., di Matteo, T., Narayan, R., & Ho, L. C., 1999, ApJ, 525, L89

Reig, P., Belloni, T., van der Klis, M., Kylafix, N., & Ford, E. C., 2000, ApJ, submitted (astro-ph/0001134)

Rutledge, R. E., Lewin, W. H. G., van der Klis, M., van Paradijs, J., Dotani, T., Vaughan, B., Belloni, T., Oosterbroek, T., & Kouveliotou, C., 1999, ApJS, 124, 265

Shakura, N. I., & Sunyaev, R. A. 1973, A&A 24, 337

Sobczak, G. J., McClintock, J. E., Remillard, R. A., Bailyn, C. D., & Orosz, J. A., 1999, ApJ, 520, 776

van der Klis, M., 1995, in X-Ray Binaries, eds. W. H. Levin, J. van Paradijs, & E. P. J. van den Heuvel (Cambridge: Cambridge Univ. Press), 252

Table 1.   Results of our Monte-Carlo simulations to reproduce the phase lag behavior of GRS 1915+105. The phase lags $\Delta\phi$ [rad] are the hard lags between channels [4] (13 – 41 keV) and [2] (3.3 – 5.8 keV).

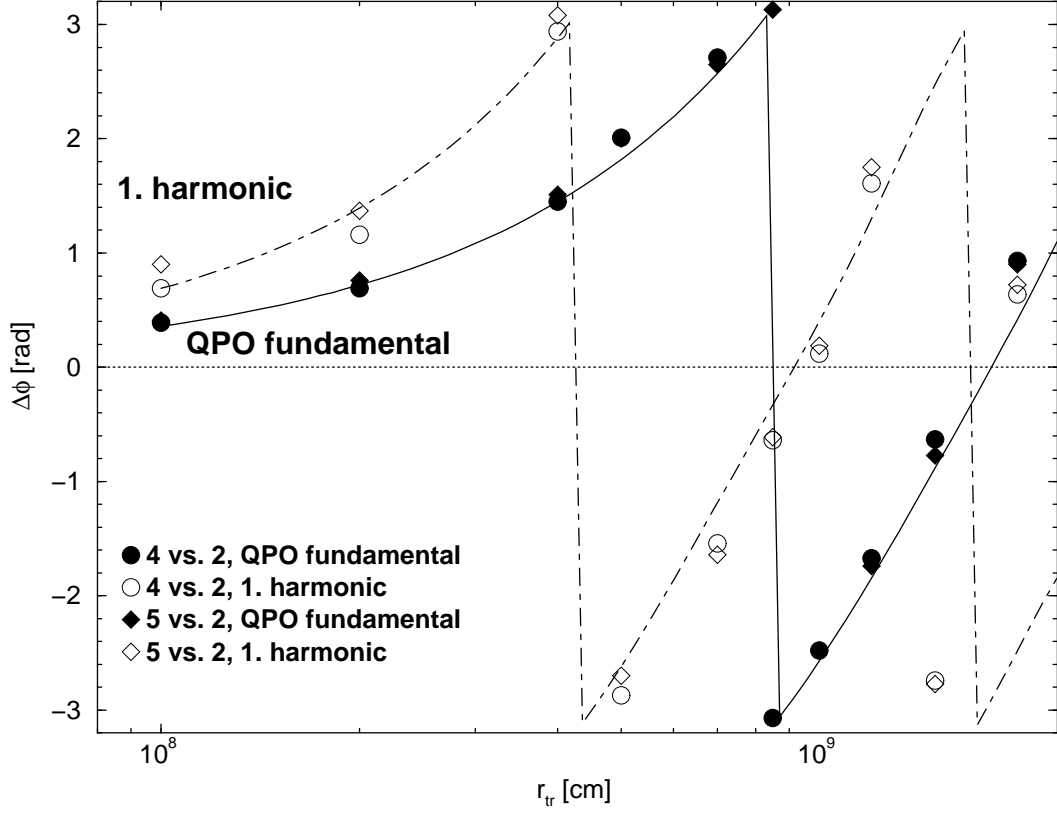| r_{tr} [cm]	f_{QPO} [Hz]	kT_{D} [keV]	$\Delta\phi_{\mathrm{QPO}}$	$\Delta\phi_{\mathrm{1.\,harm.}}$	$\Delta\phi_{\mathrm{2.\,harm.}}$
1.7×10^9	0.5	0.7	+0.11	+0.13	-0.58
1.3×10^9	1.1	0.8	+0.11	+0.20	+0.20
1.0×10^9	2.3	1.0	+0.06	+1.71	-3.13
8.0×10^8	4.4	1.2	+0.02	+2.54	-2.57
7.0×10^8	6.7	1.4	-0.13	+2.64	-2.59
6.0×10^8	10.0	1.5	-0.17	+2.54	-2.92

Fig. 1.— Comparison of the analytical estimates for the phase lags at the QPO fundamental and 1. harmonic frequencies to the results of numerical Monte-Carlo simulations. Solid curve: analytical approximation for the lag at the QPO fundamental frequency; dot-dashed curve: approximation for the lag at the 1. harmonic; filled symbols: phase lags at the QPO fundamental frequency resulting from simulations; open symbols: phase lags at the 1. harmonic from simulations. Parameters: $f_{QPO} = 10$ Hz, $\tau_T^{ADAF} = 2$, $kT_D(r_{tr}) = 0.5$ keV. The energy channels are [1] $0.1 - 2.0$ keV; [2] $2.0 - 5.4$ keV; [3] $5.4 - 15$ keV; [4] $15 - 40$ keV; [5] $40 - 100$ keV.
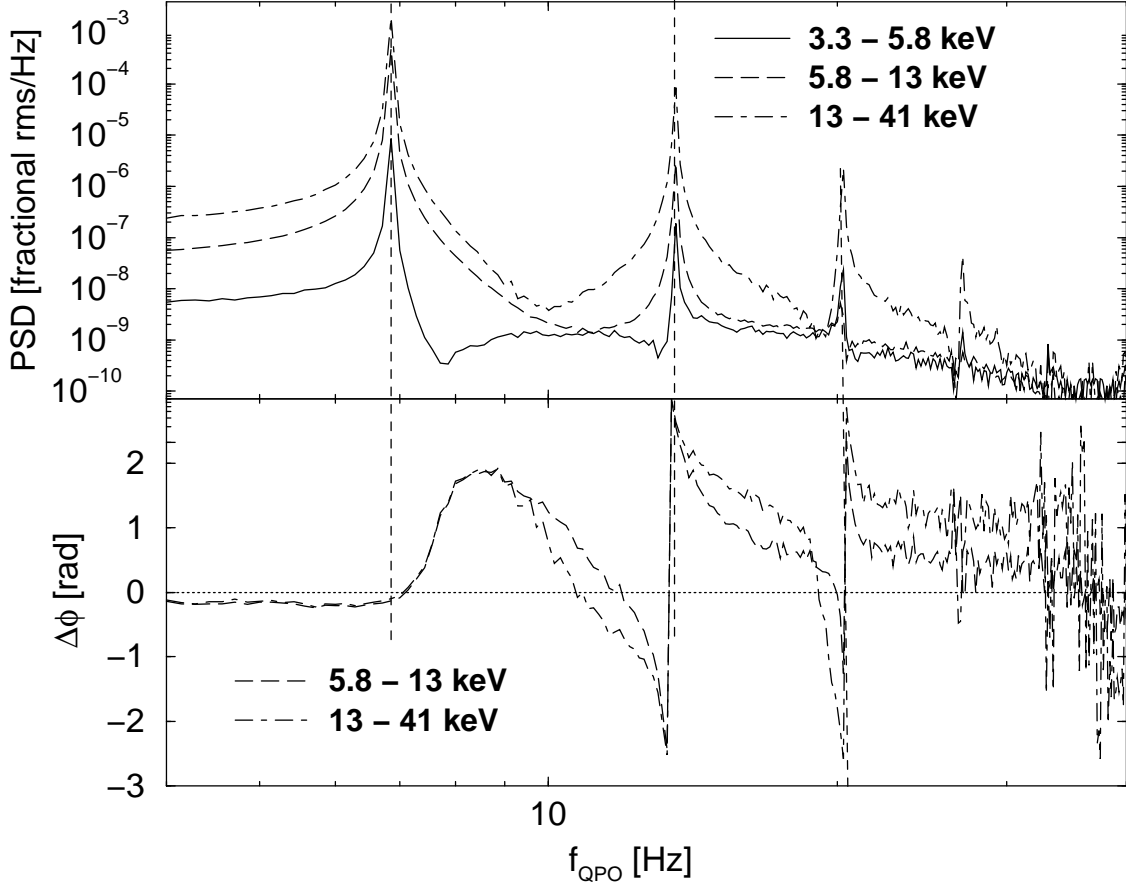
Fig. 2.— Power spectra (top panel) and phase lags with respect to the $3.3 - 5.8$ keV channel (bottom panel) of our model simulations at a high QPO frequency of $f_{\mathrm{QPO}} = 6.7$ Hz, with $r_{\mathrm{tr}} = 7 \times 10^{8}$ cm. Disk temperature: $kT_{\mathrm{D}}(r_{\mathrm{tr}}) = 1.4$ keV. Dashed vertical lines indicate the location of the QPO and its harmonics. The phase lag at the QPO fundamental frequency is negative, while the lag at the first harmonic frequency is positive. For the second harmonic, a negative lag is predicted.
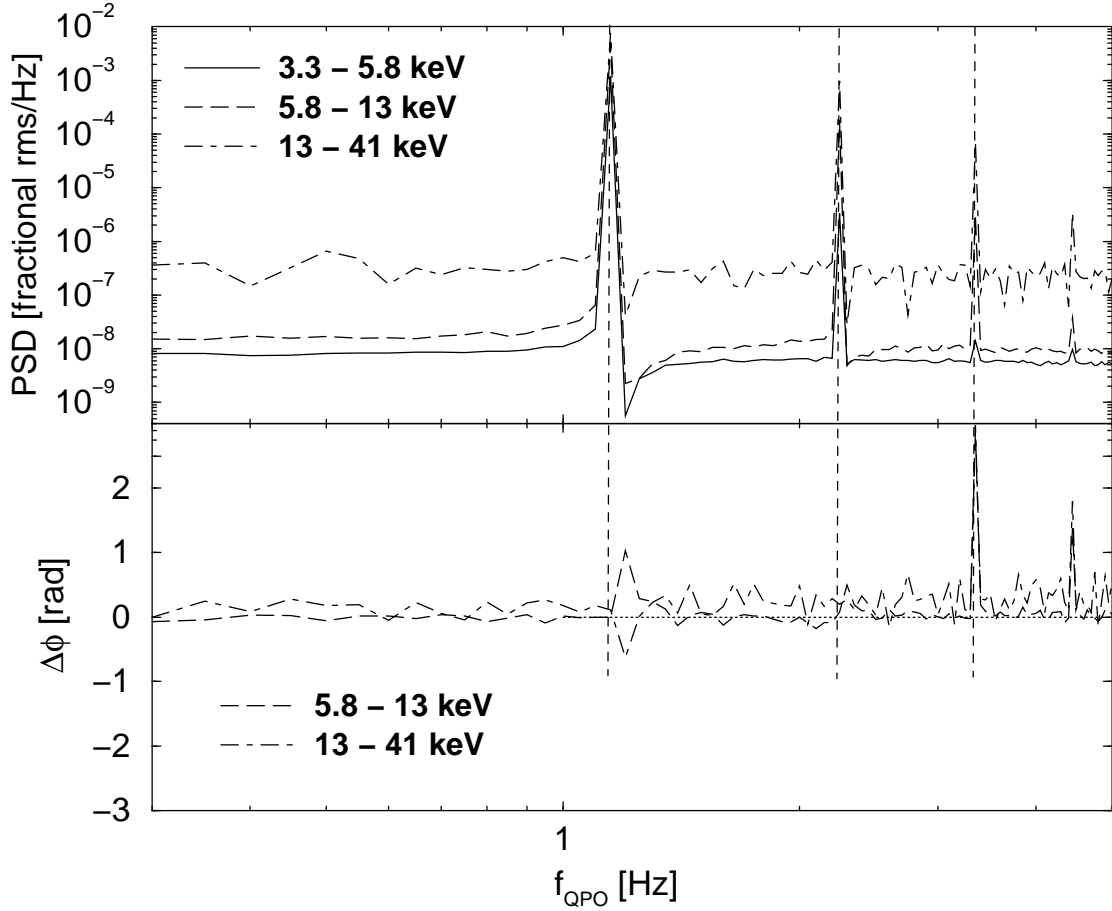
Fig. 3.— Power spectra (top panel) and phase lags with respect to the $3.3 - 5.8$ keV channel (bottom panel) of our model simulations at a low QPO frequency of $f_{\mathrm{QPO}} = 1.1$ Hz, with $r_{\mathrm{tr}} = 1.3 \times 10^9$ cm. Disk temperature: $kT_{\mathrm{D}}(r_{\mathrm{tr}}) = 0.8$ keV. Dashed vertical lines indicate the location of the QPO and its harmonics. The phase lags at both the QPO fundamental and the first harmonic frequencies are positive for the 13 - 41 keV channel. This simulation predicts a positive phase lag also at the second harmonic.
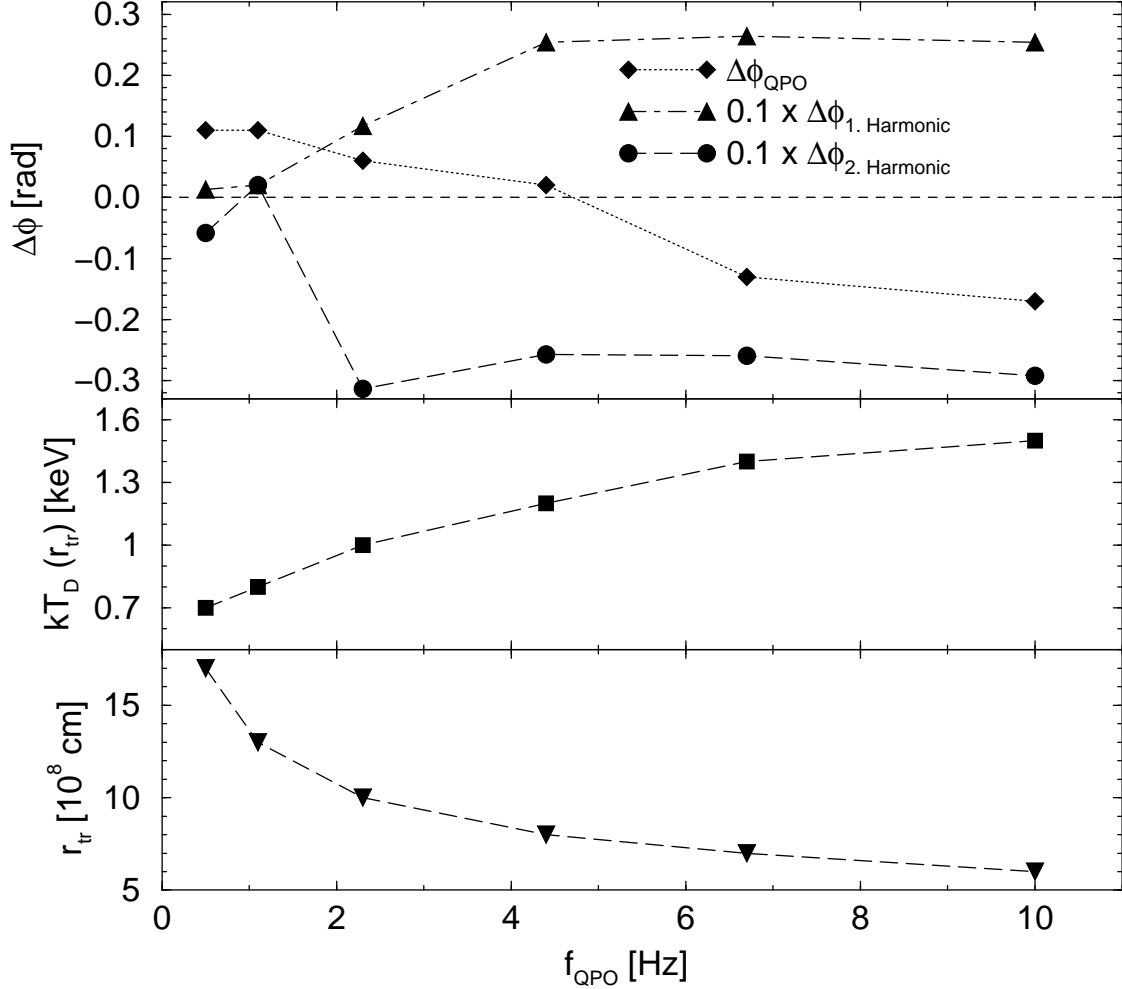
Fig. 4.— Phase lags between the 13 – 41 keV and the 3.3 – 5.8 keV energy channel at the QPO fundamental and 1. harmonic frequencies (upper panel) resulting from our Monte-Carlo simulations, with inner disk temperature as a function of QPO frequency (middle panel) determined from observations of GRS 1915+105 and disk/ADAF transition radius (lower panel) determined through $T_{\mathrm{D}}(r_{\mathrm{tr}}) \propto r_{\mathrm{tr}}^{-3/4}$. The simulations properly reproduce the changing sign of the phase lag as the QPO frequency increases, and alternating phase lags for large QPO frequencies, as observed in GRS 1915+105.